Combined effect of Mg and vacancy on the generalized planar fault energy of Al

Dongdong Zhao[a], Ole Martin Løvvik[b], Knut Marthinsen[a], and Yanjun Li[*,a]

[a]*Department of Materials Science and Engineering, Norwegian University of Science and Technology (NTNU), 7491 Trondheim, Norway*

[b]*SINTEF Materials and Chemistry, 0314 Oslo, Norway*

*Corresponding author. E-mail: yanjun.li@ntnu.no Tel.: +47 73551206

Abstract

By first-principles calculations, a systematic study has been undertaken to investigate the combined effect of vacancies and Mg impurities on the generalized planar fault energy (GPFE) of pure Al. It was predicted that introduction of a single vacancy at the stacking fault plane can decrease the GPFE and enhance twinning propensity of Al. Furthermore, vacancies were shown to exhibit a natural/activated Suzuki segregation feature towards the intrinsic/extrinsic stacking fault of Al, respectively. Along with an increasing vacancy content localized near the deformation plane a noticeable decrease in the intrinsic stacking fault energy γ_{ISFE} was obtained, which potentially may induce more split-up of dislocations into partials. However, a further increase of twinnability (based on the predicted GPFE curves) with increasing vacancy concentration was not found. More interestingly, we discovered a coupled Suzuki segregation behaviour of Mg solutes and vacancies towards the intrinsic stacking fault of Al. A systematic analysis of the twinnability parameter τ_a on basis of the modified GPFE curves under the influence of Mg solutes and vacancies clearly demonstrate the general difficulty of deformation twinning of Al-Mg alloys. Moreover, a decreased γ_{ISFE} with Mg alloying as well as with the presence of vacancies may serve, at least partially, to explain the high work-hardening rate and the formation of banded structures in Al-Mg alloys processed by severe plastic deformation (SPD).

Keywords: Generalized planar fault energy, γ_{ISFE}, Suzuki segregation, vacancy, Al-Mg alloys

1. Introduction

The Generalized Planar Fault Energy (GPFE), representing the energy penalty of rigid crystal displacements within the *fcc* (111) planes along the $<11\bar{2}>$ direction, has in recent years been widely recognized as an important descriptor for the deformation mechanisms of both coarse and nano grained *fcc* metals [1-6]. The GPFE (or γ surface) has four extrema: the unstable stacking fault energy γ_{USFE}, the intrinsic stacking fault energy γ_{ISFE}, the unstable twinning fault energy γ_{UTFE} and the twinning fault (two-layer micro twin) energy γ_{TFE}, where the latter is also referred to as the extrinsic stacking fault energy γ_{ESFE} [1, 7]. Due to the difficulties in accurate experimental measurement of these extrema [8], atomistic simulations have been widely employed to determine the GPFE, aiming to explore the atomistic mechanisms to properly analyze and interpret deformation behaviors in metals and alloys. A combination of GPFE and associated models can be used to predict and interpret many dislocation-related phenomena, e.g. emission of partial dislocations [1, 9], critical twinning stress [3], Peierls stress [10], plastic deformation regimes [1, 6], etc. For instance, following earlier works [2, 11, 12], a twinnability analysis based on the GPFE is possible, using the extensively used criterion τ_a, which is defined as a function of the number and strength of active twinning systems in terms of γ_{USFE}, γ_{ISFE} and γ_{UTFE}:

$$\tau_a = \left[1.136 - 0.151\frac{\gamma_{ISFE}}{\gamma_{USFE}}\right]\sqrt{\frac{\gamma_{USFE}}{\gamma_{UTFE}}} \tag{1}$$

Herein, a larger τ_a means stronger twinning tendency. By calculating τ_a via GPFE, an increasing propensity of Cu–Al to deform preferentially by twinning with increasing Al content has been predicted [2]. Specifically, based on relevant criteria with respect to, e.g. $\gamma_{ISFE}/\gamma_{USFE}$ and $\gamma_{UTFE}/\gamma_{USFE}$, postulated by Rice [13], Tadmor and Hai [14], the GPFE curve can be utilized to evaluate the competition between different deformation regimes like full slip and twinning. In addition, intrinsic energy barriers characterized by γ_{USFE}, γ_{USFE}-γ_{ISFE}, and γ_{UTFE}-γ_{ISFE} are widely utilized for analyzing the activation of stacking fault, twinning, and full slip. Recently, Jo et al. [6] revisited the plastic deformation mechanisms of crystalline materials by using the effective energy barriers (EEBs) on

basis of GPFE, which take into account the effect of shear directionality. Apart from this, a hierarchical, multi-scale theory in conjunction with GPFE was put forward by Kibey et al. [3] to predict the critical twinning stress τ_{crit}. Furthermore, as demonstrated in Ref. [10, 15], a coupling of GPFE and generalized Peierls-Nabarro model was able to predict the Peierls stress, which characterizes the mobility of dislocations. All these important works have proven and established the fundamental importance of GPFE in plastic deformation of crystalline materials.

Generally, most previous works have put a focus on predicting GPFE of perfect pure metals, e.g. Al, Cu, Ni, [1, 5, 16] or the effect of solute alloying on GPFE [4, 17-19]. Nevertheless, rare attention has been expended in the influence of defects, especially vacancies, upon GPFE. Vacancies, which to some extent are always present, are crucial in many material processes and reactions at the atomistic level, i.e. diffusion [20], precipitation [21, 22], segregation [23], etc. and thereby have long been known to strongly influence the properties of materials. For instance, a significant high vacancy concentration generated via severe plastic deformation (SPD) can promote grain boundary segregation of Mg solutes, thus suppressing grain growth and maintaining an ultra-fine grained (UFG) state of materials [23]. Hence, a fine control of the roles that vacancies play in these fundamental material processes can assist the engineering of special materials with desired properties. In the course of SPD at ambient temperature, vacancies are massively created due to intensive interactions of dislocations under tremendous plastic strain [23, 24]. However, to the best of the authors' knowledge, no complete and thorough theoretical work has so far been reported to address the effect of vacancy on the GPFE of Al and its alloys except for Lu and Kaxiras [25], Asadi et al. [26], both of which have confirmed theoretically that vacancies have a decreasing effect on γ_{ISFE} in Al. Using a semi-discrete variational Peierls-Nabarro model in conjunction with GPFE determined by first-principles calculations, Lu and Kaxiras [25] predicted a lubricating effect ascribed to the introduction of vacancies on the dislocation motion of Al. These interactions are considered to have strong effects upon the properties of materials [25]. It is thereby timely as well as scientifically interesting to quantify the effect of vacancy upon the GPFE of Al and its alloys. Al-Mg alloys possessing a good compromise of properties (e.g. light weight, mechanical strength, corrosion resistance etc. [23, 27]) are taken as the model system in the

present work. Experimentally, Mg solutes and vacancies are reported to be strongly coupled in an Al matrix [24], thereby the combined effect of vacancies and Mg solutes upon GPFE of Al needs to be considered.

In the first part of this work, we will study the influence of a single vacancy on the GPFE of Al. Next, the focus will be put on the effects of vacancies, in terms of local concentration and local arrangement near the deformation plane, upon the GPFE curve of Al. Hereafter, the effect of Mg-vacancy pairs and complexes upon GPFE of Al is quantified. In the last part, the special deformation behaviors of Al-Mg alloys subjected to various SPD techniques, e.g. twinnability, increased work hardening rate, planar slip of dislocations, etc. are discussed in view of the calculated effects of Mg solutes, vacancies or their combination on the GPFE of Al.

2. Computational methodology

Density functional theory with plane wave basis functions as implemented in the highly-efficient Vienna ab initio simulation package (VASP) [28, 29] was utilized for all the calculations in the present work. The core region were treated with the frozen-core projected augmented wave (PAW) method [30, 31], and the exchange–correlation functions were described with the Generalized Gradient Approximation (GGA) of Perdew–Burke–Ernzerhof (PBE) [32]. A cutoff of 350 eV employed in the present work can yield sufficiently converged results. *k*-point sampling of 13×7×1 based on the Monkhorst-Pack scheme [33] together with the linear tetrahedron method including Blöchl corrections [34] was adopted for the integration of reciprocal-space energy in the Brillouin zone (BZ). The convergence criterion of 10^{-6} eV and 10^{-4} eV were employed for the termination of electronic self-consistency and ionic loop, respectively, in the relaxation process.

A 72-atom supercell as illustrated in Fig. 1(a) was constructed in order to find the energetically favorable distributions of Mg solutes and vacancies in the Al matrix. By putting Mg solutes and vacancies at different positions (see Fig. 1(a) and Table 1), the binding energies E_b of the

vacancy-vacancy and Mg-vacancy pairs at different neighboring state in the Al matrix can be evaluated in terms of the following equations,

$$E_b\left(X-X\right)=-\left(E\left(Al_{70}X_2\right)+E\left(Al_{72}\right)-2E\left(Al_{71}X\right)\right) \quad (2)$$

$$E_b\left(X-Y\right)=-\left(E\left(Al_{70}XY\right)+E\left(Al_{72}\right)-E\left(Al_{71}X\right)-E\left(Al_{71}Y\right)\right) \quad (3)$$

where e.g. $E\left(Al_{72}\right)$ is the total electronic energy of Al_{72} as calculated by VASP, *X* is a vacancy, and *Y* is a Mg solute atom. Thus, Eq. (2) gives E_b for vacancy-vacancy pairs, while Eq. (3) for Mg-vacancy pairs. A positive E_b value corresponds to a favorable binding of the pairs. Table 1 lists the predicted E_b of the various pairs at different neighboring distances in the Al matrix. It is found that vacancies always like to stay as 2nd nearest neighbor (2nn) in the Al matrix. The repulsion between 1st nearest neighbor vacancies (1nn) and attractions as 2nn predicted by the present work are in good agreement with the calculations by Karling and Wahnström [35]. As for Mg-vacancy pairs, 4th nearest neighbors (4nn) are energetically more preferable. It is worth noting that 1nn Mg-vacancy pairs has a E_b of -0.0148 eV, which is in good agreement with the experimental value of -0.01±0.04 eV [20] and close to the LDA-produced value of -0.02 eV by Wolverton [20].

In order to calculate GPFE curves, a slab model containing a perfect stacking sequence of 12 (111) planes (ABCABCABCABC) with total 96 atoms as well as a vacuum spacing of 15 Å along the <111> direction was constructed, as shown in Fig. 1(b). Through a rigid displacement of half the crystal with respect to the other along the $<1\bar{1}2>$ direction within (111) planes (see Fig. 1 (b)), we can obtain the whole GPFE curve by calculating the energies for different configurations along the displacement path. To investigate the entire GPFE curve, two separate shear deformations of the slab model along the $<11\bar{2}>$ direction have to be enforced. Note that in each operation, the final displacement distance was $a_0/\sqrt{6}$, being the Burgers vector of a partial dislocation, with a_0 as the lattice constant of Al. As a start, a stacking fault was created through displacing the atomic layers numbered with 1–6 in one-half of the crystal (cf. Fig. 1(b)). In a second move, based on the stacking fault configuration, layers numbered from -1 to -5 in the lower part of the crystal were shifted in the

opposite direction. To attain the equilibrium state of different configurations, the atomic positions in the slab model were solely allowed to relax in the direction perpendicular to the stacking fault plane, using a conjugate-gradient relaxation algorithm. The fault energies of the different configurations along the displacement path were calculated using Eq. (4) [36, 37]:

$$E\left(\vec{f}\right)=\frac{E_{faulted}\left(\vec{f}\right)-E_{perfect}}{A} \tag{4}$$

In which, $E_{faulted}\left(\vec{f}\right)$ is the total energy of the supercell deformed by a fault vector $\vec{f}$, $E_{perfect}$ corresponds to the total energy of the perfect stacking slab, and A is the cross-section area of slab.

3. Results

3.1 Mono-vacancy effect on GPFE and Suzuki segregation of vacancies in Al

The effect of a vacancy upon the GPFE curve of Al was investigated through introducing a single vacancy ($Al_{95}Va_1$) in the stacking fault plane (layer 0 in Fig. 1(b)) residing in site 1 (see Fig. 1(e)). In this situation, an overall concentration of 1.08 at.% and a layer concentration of 12.5 at.% of vacancies is produced. The mono-vacancy affected γ_{USFE}, γ_{ISFE}, γ_{UTFE}, and γ_{TFE} of Al are summarized in Table 2, and the corresponding mono-vacancy induced GPFE curve of Al is displayed in Fig. 3, in comparison with the GPFE curves of $Al_{95}Mg_1$ as well as pure Al [38]. One can see from Fig. 3 that mono-vacancy has a more prominent decreasing effect on γ_{ISFE} of Al than that of mono-Mg solute [38], i.e. from 142.4 mJ/m^2 to 121.3 mJ/m^2, as will do for the other three extremum energy points. The vacancy mediated decrease of γ_{ISFE} in Al was also demonstrated in the theoretical works by Lu and Kaxiras [25] and Asadi et al. [26], but neither of them investigated an entire vacancy-influenced GPFE curve. Based on the analysis of GPFE curves, $Al_{95}Va_1$ was calculated to exhibit a lowered $\gamma_{ISFE}/\gamma_{USFE}$, i.e. 0.777 (see Table 2), relative to pure Al, indicating that vacancies may make the emission of partial dislocations easier. Mg ($Al_{95}Mg_1$) has previously been predicted to facilitate twinning due to an increased τ_a and decreased $\gamma_{UTFE}/\gamma_{USFE}$, γ_{UTFE}-γ_{USFE}, compared with pure Al [38]. In

this work, we find that the introduction of vacancies can also increase the twinnability τ_a of Al (τ_a = 0.909), and this promoting role is even higher than that of Mg solutes ($Al_{95}Mg_1$, τ_a = 0.904).

Suzuki segregation is an interesting phenomenon describing that impurities or vacancies are prone to segregate to stacking faults. Most previous work has focused on the Suzuki interaction between impurities and stacking fault [39, 40]. However, the Suzuki segregation of vacancies have been scarcely investigated apart from Ref. [41], in which a positive binding energy between vacancies and intrinsic stacking faults in Al was predicted from atomistic simulations using embedded atom method (EAM) potentials. This indicates that a segregation of vacancies towards intrinsic stacking faults can be expected. In order to quantify this effect, the interaction energy between a stacking fault and vacancy E_{int} was employed. It is defined as the energy difference between the stacking fault configuration with a vacancy residing in the *n*th layer relative to the fault plane and the pure stacking fault configuration [39]:

$$E_{\text{int}}^{n} = \left(E_{SF}^{Va-n} - E_{PS}^{Va}\right) - \left(E_{SF} - E_{PS}\right) \tag{5}$$

Here, E_{SF}^{Va-n} represents the total electronic energy of the stacking fault model with a vacancy residing in the *n*th layer away from the fault plane and E_{PS}^{Va} that of the perfect stacking model. E_{SF} and E_{PS} correspond to the total energies of the stacking fault and perfect stacking configurations without vacancy. Alternatively, the interaction energy E_{int}^{n} can be interpreted as the segregation energy of vacancies to the stacking fault; a negative value denotes the tendency for vacancies to segregate toward the stacking fault. Calculations reveal that E_{int}^{n} is not restricted to the stacking fault plane and has a spatial distribution in the vicinity of the fault plane. Spatially distributed E_{int}^{n} can produce a spatial concentration distribution of vacancies near the stacking fault. This layer-by-layer concentration profile of vacancies at finite temperature *T* can be calculated by employing the following equation [42]:

$$c(n) = \frac{1}{1 + \frac{1 - c_0}{c_0} \exp\left(\frac{E_{\text{int}}^n}{k_B T}\right)} \tag{6}$$

Wherein, c_0 is the nominal overall concentration of vacancies, T is the temperature, and k_B is the Boltzmann constant.

A quantified segregation of vacancies towards intrinsic and extrinsic stacking faults in Al based on Eq. (6) is presented in Fig. 3(a). The intrinsic stacking fault planes correspond to the layers labelled “0” and “1” in Fig. 1(d). It is observed in Fig. 3(a) that, similar to the Suzuki segregation of Mg in Al [38], E_{int}^n is noticeable only at a few atomic layers in the vicinity of the stacking fault plane and then diminishes at longer distances away from the fault plane. As indicated in Fig. 3(a), the effect of an intrinsic (extrinsic) stacking fault on a vacancy only extends two (three) layers. The negative E_{int}^n near the stacking fault suggests the Suzuki segregation of vacancies, either intrinsic or extrinsic. One can further find that the interaction between a vacancy and the extrinsic stacking fault is stronger than that with the intrinsic counterpart, which indicates that the vacancy is more effective in modifying the energy of extrinsic stacking faults. In spite of Suzuki segregation in Al, vacancies would behave differently in the process of approaching the fault region of intrinsic and extrinsic stacking faults. As shown in Fig. 3(a), for a vacancy getting near to an intrinsic stacking fault, energy barrier barely exists. This is consistent with the predictions by Ref. [41], which is unlike the slightly activated Suzuki segregation of Mg in Al predicted in a previous work [38]. However, in the case of approaching the extrinsic stacking fault region, vacancies would exhibit activated Suzuki segregation behavior due to the two large energy barriers on both sides of the stacking fault (layers -1 and 1 in Fig. 3(a)). We thereby conclude that the kinetic barrier is higher for vacancies to diffuse toward extrinsic stacking faults despite their higher thermodynamic stability.

The corresponding spatial concentration profile of vacancies in the vicinity of a stacking faults which was evaluated using Eq. (6) at room temperature T = 300 K is displayed in Fig. 3(b). A local enrichment of vacancies can be observed both for intrinsic and extrinsic stacking faults. Due to a

stronger interaction energy E_{int}^{n}, the highest vacancy concentration at the extrinsic stacking fault plane is much higher than that of the intrinsic counterpart. Interestingly, it is found that the spatial vacancy concentration near the intrinsic stacking fault exhibits a Gaussian-like distribution (cf. Fig. 3(b)), while the distribution is oscillatory around the extrinsic stacking fault. Furthermore, we should keep in mind that Eq. (6) is only valid at low c_0, since interactions between vacancies would become important and shall take an decisive role in controlling the local distributions near the stacking fault defect.

3.2 Vacancy concentration effects on GPFE curve of Al

As noted earlier, it is energetically favorable for vacancies to stay as 2nn in Al. Therefore, to study the effect of varying vacancy concentration on GPFE in Al, we have created models with vacancies symmetrically distributed as 2nn in the vicinity of the stacking fault plane, layer 0 in Fig. 1(c). A variety of models with 3($Al_{93}Va_3$-1, $Al_{93}Va_3$-2) and 5($Al_{91}Va_5$-1, $Al_{91}Va_5$-2) vacancies were considered, corresponding to an overall concentration of 3.1 at.% and 5.2 at.%. This is much higher than the typical equilibrium vacancy concentration in bulk materials, but can be used to evaluate the effect of different vacancy concentrations on the GPFE of Al. The detailed distribution of vacancies for these models can be found in Table 3 (Column of "Occupation") and Fig. 1(e).

Figure 4 shows the calculated GPFE curves of these models, and the corresponding GPFE data are collected in Table 3. We first note that the vacancy concentration effect on GPFE is strongly dependent on the local configurations and concentrations of vacancies in the stacking fault region. As discussed above, a single vacancy residing in the stacking fault plane can enhance twinning propensity of Al. However, no increased twinnability can be observed for the models with 3 or 5 vacancies, due to the reduced τ_a compared to that of Al (cf. Table 3). $Al_{93}Va_3$-1 and $Al_{91}Va_5$-1 have relatively lower GPFE than $Al_{93}Va_3$-2 and $Al_{91}Va_5$-2, which can be ascribed to the co-plane distribution of vacancies near the deformation plane in $Al_{93}Va_3$-1 and $Al_{91}Va_5$-1. The evolution of GPFE versus vacancy concentration are displayed in Fig. 5(a) and (b). As can be seen, the increase of vacancy concentration leads to a sustained decrease of γ_{USFE}, with accordingly, $Al_{91}Va_5$-1 has the

lowest γ_{USFE}, i.e. 125.8 mJ/m^2, which may facilitate the nucleation of leading partial dislocations and thus enhance plasticity. A maximum decrease of γ_{ISFE} down to 105.6 mJ/m^2 was obtained for $Al_{93}Va_3$-1. No further decrease of γ_{ISFE} was observed with an increasing vacancy concentration from 3.1 at.% to 5.2 at.% (as shown in Fig. 5(b)). A lowered γ_{ISFE} would increase the width of the stacking fault ribbon connecting the dissociated partial dislocations, leading to the more splitting-up of full dislocations into partials. The modified separation distance between the partials induced by vacancies calls for some caution when using transmission electron microscopy data to predict γ_{ISFE}, since the accidental introduction of vacancies due to Suzuki segregation could result in inaccurate results. The lowered GPFE due to an increased vacancy concentration are expected to facilitate the nucleation of partial and full dislocations, as well as formation of stacking faults.

3.3 The effect of combining Mg solutes and vacancies on the GPFE curves of Al

As discussed in the Introduction, during the course of severe plastic deformation, massive defects, especially vacancies, would be produced, which are generally coexisting with Mg solutes in Al-Mg alloys. The interaction between Mg solutes and vacancies might affect the GPFE curves of Al, motivating the present investigation of the combined effect of Mg solutes and vacancies on the GPFE of Al. To address this problem more systematically, we distinguish between the effect of Mg-vacancy pairs and Mg-vacancy complexes.

3.3.1 Mg-vacancy pairs

Mg-vacancy pairs were first introduced in the stacking fault plane with different neighboring distance between Mg and vacancy: 1nn ($Al_{94}Mg_1Va_1$-1nn), 3nn ($Al_{94}Mg_1Va_1$-3nn), and 4nn ($Al_{94}Mg_1Va_1$-4nn). The resulting GPFEs are listed in Table 4 and the corresponding GPFE curves are presented in Fig. 6.

Clearly, all Mg-vacancy pairs reduce the GPFE of Al significantly. As an example, the reduction in γ_{ISFE} from pairs is more significant than that of separate Mg solutes and vacancies. Besides, a correlation between the interaction energy of Mg-vacancy pairs and their effect on the GPFE of Al

can be derived by comparing Table 4 and Table 1: the shorter distance between Mg and vacancy (energetically stable), the larger reduction of the GPFE of Al. For instance, the 4nn Mg-vacancy pair with largest positive binding energy displays the smallest reduction in GPFE of Al. The correlation between the interaction energy of Mg-vacancy pairs and τ_a suggests that the more positive the binding energy in Mg-vacancy pairs, the higher propensity for twinning.

The coupled segregation effect of Mg atoms and vacancies to the fault plane is not surprising since both Mg and vacancies exhibit a Suzuki segregation feature as predicted previously. In addition, Mg atoms have a larger atomic radius than Al. Mg residing in the stacking fault plane would create lattice distortions which would drive vacancies to segregate to the stacking fault plane so as to lower the elastic strain energy. On the other hand, lattice contraction created by vacancy segregation at the stacking fault would attract the Mg atoms to diffuse to the stacking fault. The further reduction of γ_{ISFE} induced by Mg-vacancy pairs indicates that a coupled segregation of Mg and vacancy to stacking fault is more energetically favorable than having only Mg or vacancy segregation along the stacking fault.

3.3.2 Mg-vacancy complexes

The Mg-vacancy complex effect on the GPFE of Al was investigated with multi Mg and multi vacancies as ordered in the vicinity of stacking fault plane. The construction of energetically favorable Mg-vacancy complexes needs simultaneous consideration of vacancy-vacancy, Mg-vacancy interactions. Coplanar vacancy-Mg-vacancy and Mg-vacancy-Mg triplets not being in the fault plane are one kind of Mg-vacancy complex that affects the GPFE of Al. Four models with notation S1, S2, S3, and S4 were constructed (see the detailed Mg and vacancy site occupations in Table 5) to quantify the triplet effects. Figure 7(a) shows the GPFE curves under the effect of vacancy-Mg-vacancy and Mg-vacancy-Mg triplets, and the corresponding GPFE values are collected in Table 5. Clearly, both vacancy-Mg-vacancy (S1, S2) and Mg-vacancy-Mg (S3, S4) triplets lower the GPFE of Al (cf. Fig. 7a). In comparison with $Al_{95}Mg_1$ [38], S1 and S2 have further reduced GPFE, showing that the introduction of the two extra vacancies is favorable for GPFE reduction. It is, however, a different case for S3 and S4. Compared with $Al_{95}Va_1$, an introduction of two extra Mg atoms raises the GPFE

of S3, while an increased γ_{ISFE} and reduced γ_{USFE}, γ_{UTFE}, γ_{TFE} were observed for S4. Besides, the calculated $\gamma_{ISFE}/\gamma_{USFE}$, i.e. > 0.790 and τ_a, i.e. < 0.905 of S1 to S4, imply that these coplanar vacancy-Mg-vacancy and Mg-vacancy-Mg triplets do not produce high propensity for the formation of partial dislocations and twinning.

In the present work, ten more systems noted as S5-S14, listed in Table 5, were utilized to calculate the influence of other Mg-vacancy complexes on the GPFE of Al. Figure 7(b-d) display the Mg-vacancy complex affected GPFE curves of Al with corresponding GPFE summarized in Table 6. As can be seen, all these Mg-vacancy complexes have a tailoring effect on the GPFE of Al, including γ_{USFE}, γ_{ISFE}, γ_{UTFE}, and γ_{TFE}. However, no increased twinnability induced by these Mg-vacancy complexes was observed as compared to pure Al except for S9, which possesses a τ_a value of 0.900. A maximum decrease of γ_{ISFE} to 112.8 mJ/m^2 among these complexes was predicted for S14, which has one vacancy in the fault plane, and two 4nn Mg-vacancy pairs in layer 2 and -2. S11 with three 4nn Mg-vacancy pairs positioned in layer -2, 0 and 2 produced the lowest value of γ_{USFE}, i.e. 138.0 mJ/m^2 and a comparably low γ_{ISFE}, i.e. 113.9 mJ/m^2 in the complexes. This can be attributed to the fact that a 4nn Mg-vacancy pair is effective in altering the GPFE of Al, as discussed in Section 3.3.1. It is found that for complexes with vacancy residing in the stacking fault plane, a relatively lower γ_{ISFE} can be obtained, and a higher vacancy content can result in an even more reduction of GPFE (see S11, S14 in Table 5).

4. Discussion

To visualize and facilitate the discussion of the combined effect of Mg and vacancy upon the GPFE of Al, we propose an intrinsic stacking fault energy map (presented in Fig. 8) to show the variation of twinnability parameter τ_a and γ_{ISFE} of different configurations. The results of all the investigated systems in this work, including Al, $Al_{95}Va_1$, Al_xVa_y, $Al_{94}Mg_1Va_1$, and $Al_xMg_yVa_z$ complexes as well as Cu, $Al_{95}Mg_1$, Al_xMg_y from Ref. [38] are collected in this map. Additionally, two straight dot lines marking τ_a and γ_{ISFE} of pure Al have been added in the map, aiming to make direct comparison with Al.

4.1 Twinning propensity of Al-Mg alloys during plastic deformation

The systems exhibiting an increased twinnability compared to Al are marked out with a red rectangle in Fig. 8. Obviously, only a few configurations possess a higher twinning propensity than Al. It is dementrated that the local concentrations and distributions of Mg and vacancy near the stacking fault plane play crucial roles in determining whether it can promote twinning in Al. As indicated in Fig. 8, although certain concentrations and arrangement of Mg and vacancies can enhance twinning propensity of Al, the increase is generally quite limited. A maximum τ_a of 0.919 among all the Al systems has been predicted for $Al_{93}Mg_3$-1 [38], still, this value is much less than that of Cu, i.e. 1.036. If we apply the criterion that τ_a value being larger than unity would indicate twinning [12, 43], then all the Al systems considered in this work can be predicted as "unlikely to deform by twinning". This can explain the fact that deformation twinning has been scarcely reported in the Al-Mg alloys, even subjected to various severe plastic deformation techniques including equal-channel angular pressing (ECAP) [44-46], high pressure torsion (HPT) [23], dynamic plastic deformation (DPD) [27], et al. However, as reported, deformation twinning can be promoted by high strain rate, lower temperature, etc. [47, 48]. Thus, in spite of the low τ_a value, twinning of Al-Mg alloys can still be expected under certain extreme conditions. For instance, Gray [49] observed deformation twinning in Al–4.8 wt.% Mg subjected to shock loading (strain rate ~10^7 s^{-1}) at a low temperature of -180°C. In addition, grain size would be another factor that affects deformation twinning in materials, i.e. the inverse grain-size effect [47]. In view of this effect, Liao et al. [50] reported deformation twinning in an Al–7.6 at.% Mg alloy processed by cryogenic ball-milling with the grain size less than 10 nm. However, the factors affecting deformation twinning under these extreme conditions are beyond the scope and prediction capabilities of the present work.

4.2 Influence of reduced γ_{ISFE} in Al-Mg alloys on recrystallization

Al-Mg alloys subjected to SPD are reported to have a high dislocation density and high work-hardening rate [23, 44, 45], which have been attributed to the Mg alloying [23, 44, 45]. It is discussed that a suppressed dynamic recovery tendency plays an important role in maintaining the high

dislocation density and high work-hardening rate of Al-Mg alloys at larger strains [45]. As a matter of fact, the dynamic recovery suppression in SPD processed Al-Mg alloys can be partially attributed to the reduction of γ_{ISFE}. It is widely known that to eliminate elastic energy, full dislocations in *fcc* metals and alloys usually split up into two Shockley partial dislocations through the dislocation reaction $\frac{1}{2}[1\bar{1}0] \rightarrow \frac{1}{6}[1\bar{2}1] + \frac{1}{6}[2\bar{1}\bar{1}]$ [51], with a stacking fault ribbon connecting the two partials. The width of the stacking fault ribbon depends on γ_{ISFE} and may significantly influence the dislocation mobility. Generally, the two partial dislocations have to be joined together before a dislocation can cross-slip to an adjacent plane [52]. Hence, in low γ_{ISFE} materials possessing wider stacking fault ribbon, cross-slip of full dislocations is relatively more difficult, leading to suppressed dynamic recovery and thus high work-hardening rate during plastic deformation [16]. As indicated in by the blue rectangle in Fig. 8, one can find that Mg solutes, vacancies, as well as Mg-vacancy pairs and/or complex can all reduce the value of γ_{ISFE} of Al, which is an indication that Al-Mg alloys in general would exhibit a lower γ_{ISFE} than pure Al, being in good agreement with experimental results [53]. During SPD processing, more vacancies and Mg-vacancy pairs/complex can be introduced in Al-Mg alloys, which would further reduce γ_{ISFE}, resulting in further suppressed dynamic recovery and thus enhanced work-hardening rate.

Al-Mg alloys with a high Mg content have been reported to show planar glide deformation characteristics [54, 55]. As suggested by Hong et al. [56], γ_{ISFE} imposes a crucial influence upon the planarity of dislocation movement. Usually in materials with high γ_{ISFE}, for instance Al, dislocations have three-dimensional mobility and can easily cross slip [57], due to the small separation distances between the partial dislocations. Extensive cross slip of dislocations would make these materials exhibit a wavy glide behavior [56], which facilitates the formation of a heterogeneous distribution of dislocations, i.e. dislocation tangling, clustering or cell structures. A decrease in γ_{ISFE} can help to bind the dislocations to their respective slip planes, thus promoting planar glide of dislocations. Besides, stacking faults connecting the partials will cover a geometrical region and have repulsions between each other. The width of the stacking fault region is inversely proportional to γ_{ISFE}: with a smaller γ_{ISFE}, a larger stacking fault region can be expected. The short range repulsions between these stacking fault

regions will restrain the clustering of dislocations [56]. Consequently, a decrease of γ_{ISFE} shall enhance the extent of planar slip of dislocations, which would facilitate the formation of banded structures (slip band, deformation band) in the process of deformation. Thereby the case of formation of banded structures in the SPD processed Al-Mg alloys can be partially explained by a decreased γ_{ISFE} resulting from Mg alloying and vacancies. However, it has to be noted that the planar slip of dislocations in the SPD processed Al-Mg alloys is not only associated with the decreased γ_{ISFE}, as the reduction of γ_{ISFE} predicted in the current work is still limited. Since Al-Mg alloys possess a comparable shear modulus with Al, the promotion of planar slip behavior in the SPD processed Al-Mg alloys should also be attributed to the enhanced friction stress induced by the interactions between Mg solutes and dislocations [55, 58, 59], as well as atomic size misfit, which need further investigations.

5. Conclusion

A systematic first-principles study has been conducted to investigate the combined effect of vacancies and Mg solutes on the GPFE of Al. It is found that a single vacancy residing in the stacking fault plane (plane concentration 12.5 at.%) can decrease the GPFE and increase twinnablility of Al. As predicted, the natural Suzuki segregation of vacancy towards the intrinsic stacking fault gives rise to a Gaussian-like concentration distribution in the vicinity of intrinsic stacking faults in Al. It follows that an increasing vacancy concentration can produce a considerable decrease in γ_{ISFE} of Al. However, no further increase of twinning propensity was observed when introducing more vacancies. One interesting phenomenon predicted in the present work is the coupled segregation of vacancies and Mg towards intrinsic stacking faults in Al, i.e. the Suzuki segregation of Mg and vacancies to stacking faults are mutually stimulated. Finally, the twinnability analysis based on the modified GPFE of Al by introduction of vacancies and Mg atoms signifies the general difficulty of deformation twinning in Al-Mg alloys, consistent with the rarely reported deformation twin forming in coarse grained Al-Mg alloys even subjected to various SPD strategies. Nevertheless, a reduction in γ_{ISFE} attributed to Mg and vacancy introduction can, at least partially, explain the high work-hardening rate and the formation of banded structures in SPD processed Al-Mg alloys.

Acknowledgements

This work is financially supported under the FRINATEK project 'BENTMAT' (project number 222173) from Research Council of Norway. Computation time from the NOTUR consortium is gratefully acknowledged.

References

[1] H.V. Swygenhoven, P.M. Derlet, A.G. Frøseth, Stacking fault energies and slip in nanocrystalline metals, Nature Mater., 3 (2004) 399-403.

[2] S. Kibey, J. B. Liu, D. D. Johnson, H. Sehitoglu, Generalized planar fault energies and twinning in Cu-Al alloys, Appl. Phys. Lett., 89 (2006) 191911.

[3] S. Kibey, J.B. Liu, D.D. Johnson, H. Sehitoglu, Predicting twinning stress in fcc metals: Linking twin-energy pathways to twin nucleation, Acta. Mater., 55 (2007) 6843-6851.

[4] M. Muzyk, Z. Pakiela, K.J. Kurzydlowski, Ab initio calculations of the generalized stacking fault energy in aluminium alloys, Scr. Mater., 64 (2011) 916-918.

[5] S.L. Shang, W.Y. Wang, Y. Wang, Y. Du, J.X. Zhang, A.D. Patel, Z.K. Liu, Temperature-dependent ideal strength and stacking fault energy of fcc Ni: a first-principles study of shear deformation, J. Phys.: Condens. Matter, 24 (2012) 155402.

[6] M. Jo, Y.M. Koo, B.-J. Lee, B. Johansson, L. Vitos, S.K. Kwon, Theory for plasticity of face-centered cubic metals, PNAS, 111 (2014) 6560–6565.

[7] D.J. Siegel, Generalized stacking fault energies, ductilities, and twinnabilities of Ni and selected Ni alloys, Appl. Phys. Lett., 87 (2005) 121901.

[8] S.L. Shang, C.L. Zacherl, H.Z. Fang, Y. Wang, Y. Du, Z.K. Liu, Effects of alloying element and temperature on the stacking fault energies of dilute Ni-base superalloys, J. Phys.: Condens. Matter, 24 (2012) 505403.

[9] H. Hu, X. Wu, R. Wang, Z. Jia, W. Li, Q. Liu, Structural stability, mechanical properties and stacking fault energies of $TiAl_3$ alloyed with Zn, Cu, Ag: First-principles study, J. Alloys. Comp., 666 (2016) 185-196.

[10] G. Lu, N. Kioussis, V.V. Bulatov, E. Kaxiras, Generalized-stacking-fault energy surface and dislocation properties of aluminum, Phys. Rev. B, 62 (2000) 3099-3108.

[11] E.B. Tadmora, N. Bernstein, A first-principles measure for the twinnability of FCC metals, J. Mech. Phys. Solids, 52 (2004) 2507–2519.

[12] N. Bernstein, E. B. Tadmor, Tight-binding calculations of stacking energies and twinnability in fcc metals, Phys. Rev. B, 69 (2004) 094116.
[13] J.R. Rice, Dislocation nucleation from a crack tip an analysis based on the peierls concept, J. Mech. Phys. Solids., 40 (1992) 239-271.
[14] E.B. Tadmor, S. Hai, A Peierls criterion for the onset of deformation twinning at a crack tip, J. Mech. Phys. Solids., 51 (2003) 765–793.
[15] J. Hartford, B. von Sydow, G. Wahnström, B.I. Lundqvist, Peierls barriers and stresses for edge dislocations in Pd and Al calculated from first principles, Phys. Rev. B, 58 (1998) 2487-2496.
[16] M. Bhogra, U. Ramamurty, U.V. Waghmare, Temperature-dependent stability of stacking faults in Al, Cu and Ni: first-principles analysis, J. Phys.: Condens. Matter, 26 (2014) 385402.
[17] M. Muzyk, Z. Pakielaa, K.J. Kurzydlowski, Generalized stacking fault energy in magnesium alloys: Density functional theory calculations, Scr. Mater., 66 (2012) 219-222.
[18] C. Wang, H. Zhang, H. Wang, G. Liu, Q. Jiang, Effects of doping atoms on the generalized stacking-fault energies of Mg alloys from first-principles calculations, Scr. Mater., 69 (2013) 445-448.
[19] N.I. Medvedeva, M.S. Park, D.C. Van Aken, J.E. Medvedeva, First-principles study of Mn, Al and C distribution and their effect on stacking fault energies in fcc Fe, J. Alloys. Comp., 582 (2014) 475-482.
[20] C. Wolverton, Solute–vacancy binding in aluminum, Acta Mater, 55 (2007) 5867–5872.
[21] E. Ozawa, H. Kimura, Excess vacancies and the nucleation of precipitates in Aluminium-Silicon alloys, Acta. Metall., 18 (1970) 995-1004.
[22] F. Soisson, C.C. Fu, Cu-precipitation kinetics in α-Fe from atomistic simulations: Vacancy-trapping effects and Cu-cluster mobility, Phys. Rev. B, 76 (2007) 214102.
[23] X. Sauvage, N. Enikeev, R. Valiev, Y. Nasedkina, M. Murashkin, Atomic-scale analysis of the segregation and precipitation mechanisms in a severely deformed Al–Mg alloy, Acta Mater, 72 (2014) 125–136.
[24] X. Sauvage, A. Ganeev, Y. Ivanisenko, N. Enikeev, M. Murashkin, R. Valiev, Grain Boundary Segregation in UFG Alloys Processed by Severe Plastic Deformation, Adv. Eng. Mater., 14 (2012) 968-974.
[25] G. Lu, E. Kaxiras, Can Vacancies Lubricate Dislocation Motion in Aluminum?, Phys. Rev. Lett., 89 (2002) 105501.
[26] E. Asadi, M.A. Zaeem, A. Moitra, M.A. Tschopp, Effect of vacancy defects on generalized stacking fault energy of fcc metals, J. Phys.: Condens. Matter, 26 (2014) 115404.
[27] S. Jin, N. Tao, K. Marthinsen, Y. Li, Deformation of an Al–7Mg alloy with extensive structural micro-segregations during dynamic plastic deformation, Mater. Sci. Eng. A, 628 (2015) 160–167.
[28] G. Kresse, J. Furthmiiller, Efficiency of ab-initio total energy calculations for metals and semiconductors using a plane-wave basis set, Comp. Mater. Sci., 6 (1996) 15-50.

[29] G. Kresse, J. Furthmüller, Efficient iterative schemes for ab initio total-energy calculations using a plane-wave basis set, Phys. Rev. B, 54 (1996) 11169-11186.
[30] P.E. Blöchl, Projector augmented-wave method, Phys. Rev. B, 50 (1994) 17953-17979.
[31] G. Kresse, D. Joubert, From ultrasoft pseudopotentials to the projector augmented-wave method, Phys. Rev. B, 59 (1999) 1758-1775.
[32] J.P. Perdew, K. Burke, M. Ernzerhof, Generalized Gradient Approximation Made Simple, Phys. Rev. Lett., 77 (1996) 3865.
[33] H.J. Monkhorst, J.D. Pack, Special points for Brillouin-zone integrations, Phys. Rev. B, 13 (1976) 5188-5192.
[34] P.E. Blöchl, O. Jepsen, O.K. Andersen, Improved tetrahedron method for Brillouin-zone integrations, Phys. Rev. B, 49 (1994) 16223-16233
[35] K. Carling, G. Wahnström, Vacancies in Metals: From First-Principles Calculations to Experimental Data, Phys. Rev. Lett., 85 (2000) 3862.
[36] C. Wang, H. Wang, T. Huang, X. Xue, F. Qiu, Q. Jiang, Generalized-stacking-fault energy and twin-boundary energy of hexagonal close-packed Au: A firstprinciples calculation, Sci. Rep., 5 (2015) 10213.
[37] C. Wang, H. Wang, H. Zhang, X. Nan, E. Xue, Q. Jiang, First-principles study of generalized-stacking-fault (GSF) energy in Mg with Al and Zn alloyings, J. Alloys. Comp., 575 (2013) 423-433.
[38] D.D. Zhao, O.M. Løvvik, K. Marthinsen, Y.J. Li, Impurity effect of Mg on the generalized planar fault energy of Al, J. Mater. Sci., 51 (2016) 6552–6568.
[39] T. Fan, L. Wei, B. Tang, L. Peng, W. Ding, Effect of temperature-induced solute distribution on stacking fault energy in Mg–X(X = Li, Cu, Zn, Al, Y and Zr) solid solution: a first-principles study, Phil. Mag., 94 (2014) 1578–1587.
[40] X.-Y. Cui, H.-W. Yen, S.-Q. Zhu, R. Zheng, S.P. Ringer, On the universality of Suzuki segregation in binary Mg alloys from first principles, J. Alloys. Comp., 620 (2015) 38–41.
[41] E. Clouet, The vacancy–edge dislocation interaction in fcc metals: A comparison between atomic simulations and elasticity theory, Acta Mater., 54 (2006) 3543–3552.
[42] E. Dontsova, J. Rottler, C.W. Sinclair, Solute-defect interactions in Al-Mg alloys from diffusive variational Gaussian calculations, Phys. Rev. B, 90 (2014) 174102.
[43] A. Hunter, I.J. Beyerlein, Relationship between monolayer stacking faults and twins in nanocrystals, Acta Mater, 88 (2015) 207–217.
[44] M. Zha, Y. Li, R.H. Mathiesen, R. Bjørge, H.J. Roven, Achieve high ductility and strength in an Al–Mg alloy by severe plastic deformation combined with inter-pass annealing, Mater. Sci. Eng. A, 598 (2014) 141–146.
[45] M. Zha, Y. Li, R.H. Mathiesen, R. Bjørge, H.J. Roven, Microstructure evolution and mechanical behavior of a binary Al–7Mg alloy processed by equal-channel angular pressing, Acta Mater, 84 (2015) 42–54.

[46] D.G. Morris, M.A. Munoz-Morris, Microstructure of severely deformed Al–3Mg and its evolution during annealing, Acta Mater., 50 (2002) 4047–4060.
[47] Y.T. Zhu, X.Z. Liao, X.L. Wu, Deformation twinning in nanocrystalline materials, Prog. Mater. Sci., 57 (2012) 1-62.
[48] J.W. Christian, S. Mahajant, Deformation twinning, Prog. Mater. Sci., 39 (1995) 1-157.
[49] G.T. Gray, Deformation twinning in Al-4.8 wt% Mg, Acta metall., 36 (1988) 1745-1754.
[50] X.Z. Liao, J.Y. Huang, Y.T. Zhu, Nanostructures and deformation mechanisms in a cryogenically ball-milled Al–Mg alloy, Phil. Mag., 83 (2003) 3065–3075.
[51] M. Jahnátek, J. Hafner, M. Krajčí, Shear deformation, ideal strength, and stacking fault formation of fcc metals: A density-functional study of Al and Cu, Phys. Rev. B, 79 (2009) 224103.
[52] Y. Qi, R.K. Mishra, Ab initio study of the effect of solute atoms on the stacking fault energy in aluminum, Phys. Rev. B, 75 (2007) 224105.
[53] M.S. Soliman, The high-temperature creep behaviour of an AI-1 wt% Cu solid-solution alloy, J. Mater. Sci., 28 (1993) 4483-4488.
[54] B. Bay, N. Hansen, D.A. Hughes, D. Kuhlmann-Wilsdorp, Evolution of f.c.c deformation structures in polyslip, Acta Metall. Mater., 40 (1992) 205-219.
[55] D.A. Hughes, Microstructural evolution in a non-cell forming metal: Al-Mg, Acta Metall. Mater., 41 (1993) 1421-1430.
[56] S.I. Hong, C. Laird, Mechanisms of slip mode modification in f.c.c. solid solutions, Acta Metall. Mater., 38 (1990) 1581-1594.
[57] D. Kuhlmann-Wilsdorf, The connection between recovery and glide type in Aluminum and Al-Mg, Mater. Sci. Forum, 331-337 (2000) 689-702.
[58] B. Bay, N. Hansen, D.A. Hughes, D. Kuhlmann-Wilsdorf, Evolution of F.C.C. deformation structures in polyslip, Acta metall, mater., 40 (1992) 205-219.
[59] D. Kuhlmann-Wilsdorf, Theory of Plastic Deformation:-- properties of low energy dislocation structures, Mater. Sci. Eng. A, 3 (1989) 1-41.

Tables

Table 1. Binding energy E_b (eV) for the Mg-Mg, vacancy-vacancy, and Mg-vacancy pairs as function of their separation distance in the Al matrix. A positive value indicates a favorable binding state. The occupations of Mg or vacancy in the Al matrix as different neighbors are as indicated in Fig. 1(a).

Occupations	Neighbors	Va-Va	Mg-Va
1-2	1nn	-0.0642	-0.0148
1-3	2nn	0.0173	0.0031
1-4	3nn	0.0049	-0.0040
1-5	4nn	0.0159	0.0187
1-6	5nn	0.0038	-0.0103

Table 2. Mono-Mg and mono-vacancy effect on unstable stacking fault energy γ_{USFE}, stacking fault energy γ_{ISFE}, unstable twinning fault energy γ_{UTFE} and twinning fault energy γ_{TFE} of Al. The energies are in mJ/m^2.

System	γ_{USFE}	γ_{ISFE}	γ_{UTFE}	$2\gamma_{TFE}$	$\gamma_{ISFE}/\gamma_{USFE}$	$\gamma_{UTFE}/\gamma_{USFE}$	$\gamma_{UTFE}-\gamma_{USFE}$	τ_a (Twinnability)
[a]Al_{96}	177.4	142.4	226.5	135.4	0.803	1.277	49.1	0.898
[a]$Al_{95}Mg_1$	168.0	135.0	211.6	119.1	0.804	1.260	43.6	0.904
$Al_{95}Va_1$	156.2	121.3	196.0	102.5	0.777	1.255	39.8	0.909

[a]Data from Ref. [38].

Table 3. Vacancy concentration effect on unstable stacking fault energy γ_{USFE}, stacking fault energy γ_{ISFE}, unstable twinning fault energy γ_{UTFE} and twinning fault energy γ_{TFE} of Al. The energies are in mJ/m^2. The subscript number in the "Occupation" column corresponds to the atomic positions as indicated in Fig. 1(c) for possible vacancy substitutions.

System	Occupation	γ_{USFE}	γ_{ISFE}	γ_{UTFE}	$2\gamma_{TFE}$	$\gamma_{ISFE}/\gamma_{USFE}$	$\gamma_{UTFE}/\gamma_{USFE}$	$\gamma_{UTFE}-\gamma_{USFE}$	τ_a (Twinnability)
Al_{96}	-	177.4	142.4	226.5	135.4	0.803	1.277	49.1	0.898
$Al_{93}Va_3$-1	$Va_{(1,5,7)}$	131.0	105.6	171.3	106.3	0.806	1.307	40.3	0.887
$Al_{93}Va_3$-2	$Va_{(1,8,6)}$	140.1	108.8	208.2	132.4	0.777	1.486	68.1	0.836
$Al_{91}Va_5$-1	$Va_{(1,5,7,9,11)}$	125.8	109.8	172.0	107.4	0.872	1.367	46.2	0.859
$Al_{91}Va_5$-2	$Va_{(1,5,7,10,12)}$	152.9	125.5	196.4	117.1	0.821	1.285	43.5	0.893

Table 4. The effect of Mg and vacancy pairs on unstable stacking fault energy γ_{USFE}, stacking fault energy γ_{ISFE}, unstable twinning fault energy γ_{UTFE} and twinning fault energy γ_{TFE} of Al. Both Mg and vacancy are placed in the stacking fault plane. The subscript number in the "Occupation" column corresponds to the atomic positions as indicated in Fig. 1(e) for possible Mg or vacancy substitutions. The energies are in mJ/m^2.

System	Occupation	γ_{USFE}	γ_{ISFE}	γ_{UTFE}	$2\gamma_{TFE}$	$\gamma_{ISFE}/\gamma_{USFE}$	$\gamma_{UTFE}/\gamma_{USFE}$	$\gamma_{UTFE}-\gamma_{USFE}$	τ_a (Twinnability)
Al_{96}	-	177.4	142.4	226.5	135.4	0.803	1.277	49.1	0.898
$Al_{94}Mg_1Va_1$-1nn	$Mg_{(1)}Va_{(2)}$	135.0	107.6	174.4	91.9	0.797	1.292	39.5	0.893
$Al_{94}Mg_1Va_1$-3nn	$Mg_{(1)}Va_{(3)}$	148.7	116.2	184.8	92.1	0.782	1.243	36.1	0.913
$Al_{94}Mg_1Va_1$-4nn	$Mg_{(1)}Va_{(4)}$	153.8	119.5	189.2	92.3	0.777	1.230	35.4	0.918

Table 5. Mg and vacancy complex effect on unstable stacking fault energy γ_{USFE}, stacking fault energy γ_{ISFE}, unstable twinning fault energy γ_{UTFE} and twinning fault energy γ_{TFE} of Al. The energies are in mJ/m^2. The subscript number in the "Occupation" column corresponds to the atomic positions as indicated in Fig. 1(e) for possible Mg or vacancy substitutions.

System	Occupation	γ_{USFE}	γ_{ISFE}	γ_{UTFE}	$2\gamma_{TFE}$	$\gamma_{ISFE}/\gamma_{USFE}$	$\gamma_{UTFE}/\gamma_{USFE}$	$\gamma_{UTFE}-\gamma_{USFE}$	τ_a (Twinnability)
Al_{96}	-	177.4	142.4	226.5	135.4	0.803	1.277	49.1	0.898
S1	$Mg_{(1)}Va_{(9,11)}$	160.1	126.7	203.6	108.1	0.791	1.272	43.5	0.901
S2	$Mg_{(1)}Va_{(10,12)}$	153.9	125.0	193.7	101.9	0.812	1.258	39.8	0.903
S3	$Mg_{(9,11)}Va_{(1)}$	156.3	124.9	202.1	106.1	0.799	1.293	45.8	0.893
S4	$Mg_{(10,12)}Va_{(1)}$	153.1	123.6	193.9	97.3	0.807	1.267	40.9	0.901
S5	$Mg_{(9,10,11,12)}Va_{(1)}$	155.7	128.9	206.7	108.3	0.828	1.328	51.0	0.877
S6	$Mg_{(1,4)}Va_{(9,11)}$	158.5	131.4	204.1	113.9	0.829	1.288	45.6	0.891
S7	$Mg_{(1,4,10,12)}Va_{(9,11)}$	166.3	140.8	221.0	120.9	0.846	1.329	54.7	0.875
S8	$Mg_{(1,9,11)}Va_{(4)}$	152.0	125.4	193.1	95.7	0.825	1.270	41.1	0.898
S9	$Mg_{(1,10,12)}Va_{(4)}$	157.8	125.0	201.3	102.4	0.792	1.276	43.6	0.900
S10	$Mg_{(1,9,10,11,12)}Va_{(4)}$	157.5	130.6	212.0	112.2	0.829	1.346	54.5	0.871
S11	$Mg_{(1,9,11)}Va_{(4,10,12)}$	138.0	113.9	195.2	105.3	0.825	1.415	57.2	0.850
S12	$Mg_{(1,9,11)}Va_{(10,12)}$	155.7	131.6	200.8	101.7	0.845	1.290	45.1	0.888
S13	$Mg_{(1,10,12)}Va_{(9,11)}$	165.1	132.0	212.7	107.1	0.800	1.288	47.5	0.895
S14	$Mg_{(10,12)}Va_{(1,9,11)}$	143.9	112.8	198.1	96.5	0.784	1.377	54.3	0.867

Figures.

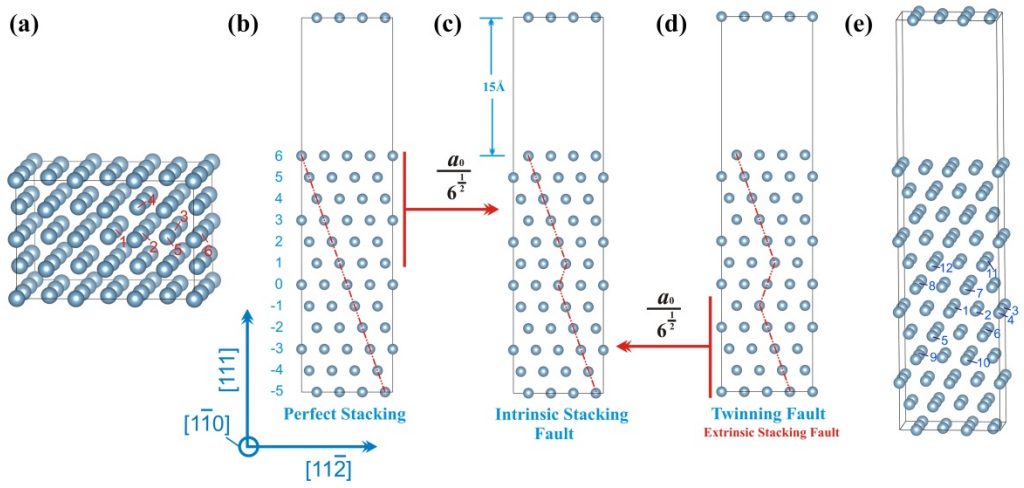

Fig. 1. (a) Indication of the positions for substitution of Mg and vacancy as different neighbors in Al matrix. Typical atomic configurations adopted in the present calculations including the perfect stacking (b), intrinsic stacking fault (c), and twinning fault configurations (d), a 15Å thickness of vacuum was implemented in all the slab models. The displacement path of the GPFE along the $<11\bar{2}>$ direction is also illustrated. (e) Atomic positions (indicated as 1-12) for possible Mg or vacancy substitutions to evaluate its effect on the GPFE of Al.

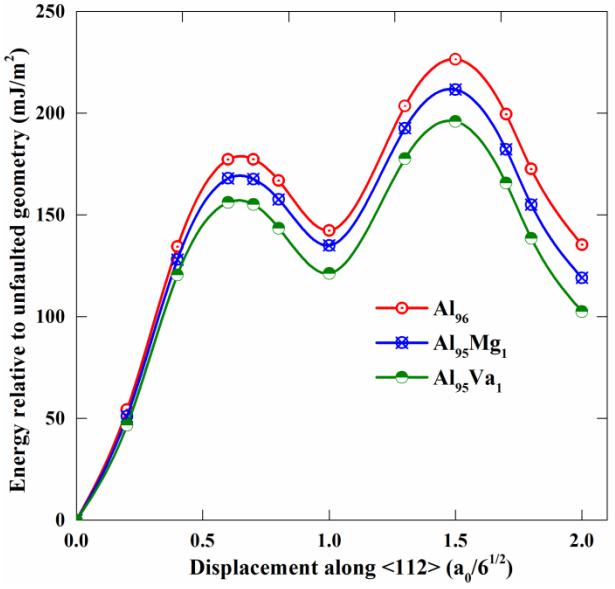

Fig. 2. Mono-vacancy effect on the GPFE curves of Al, in comparison with the GPFE curves of $Al_{95}Mg_1$ as well as pure-Al [38].

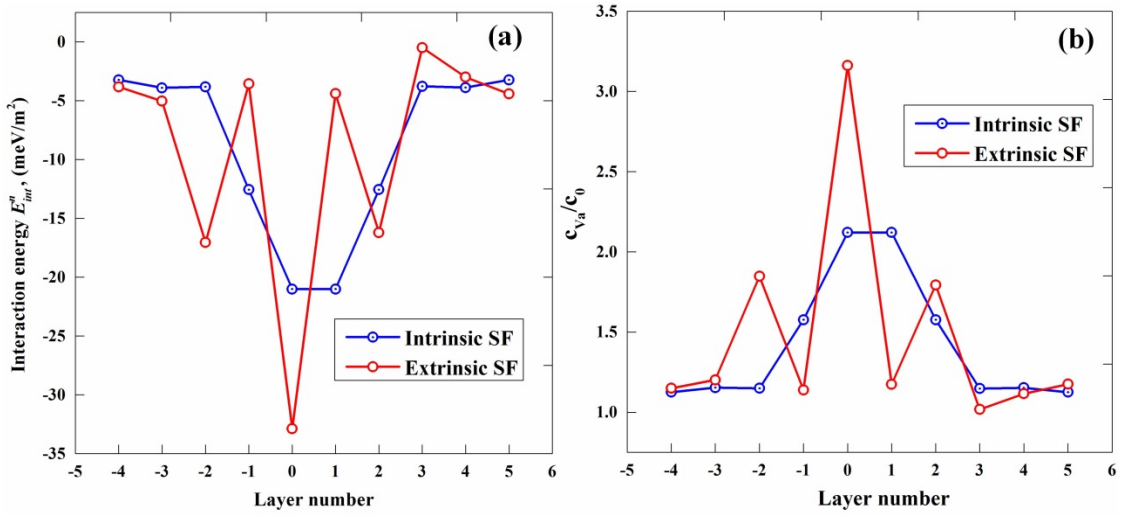

Fig. 3. (a) The interaction energy E^n_{int} (Eq. 5) between single vacancy and intrinsic (dotted circles) or extrinsic (open circles) stacking faults in Al, as a function of distance to the stacking fault, in number of atomic layers n (Fig. 1 (c) and (d)). (b) The corresponding concentration profile of vacancies c_{Va} evaluated from Eq. (6) at temperature T=300 K.

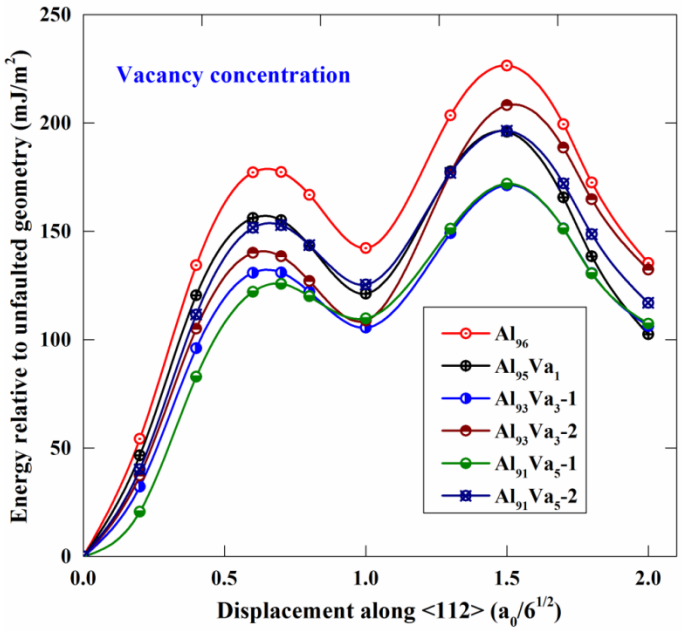

Fig. 4. Vacancy concentration effect on the GPFE curves of Al. For the detailed vacancy distributions in the vicinity of the fault plane, please refer to Table. 3.

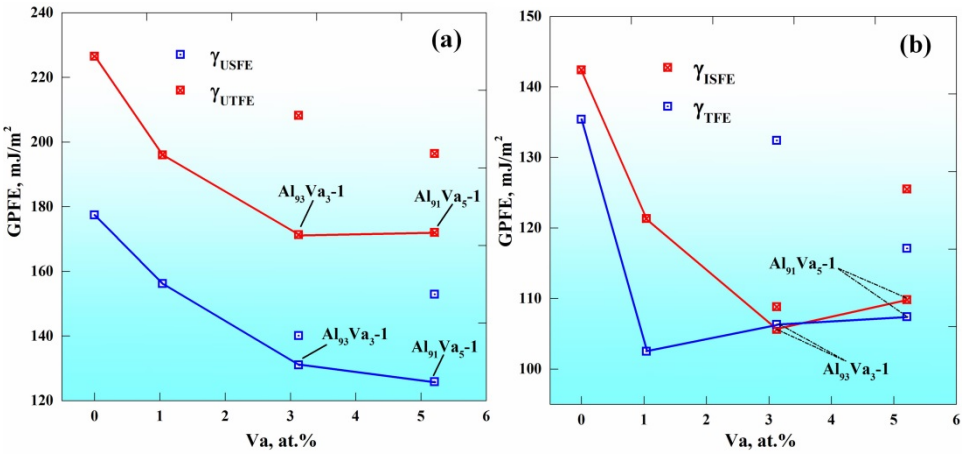

Fig. 5. Variation of the GPFE values of Al versus vacancy concentration.

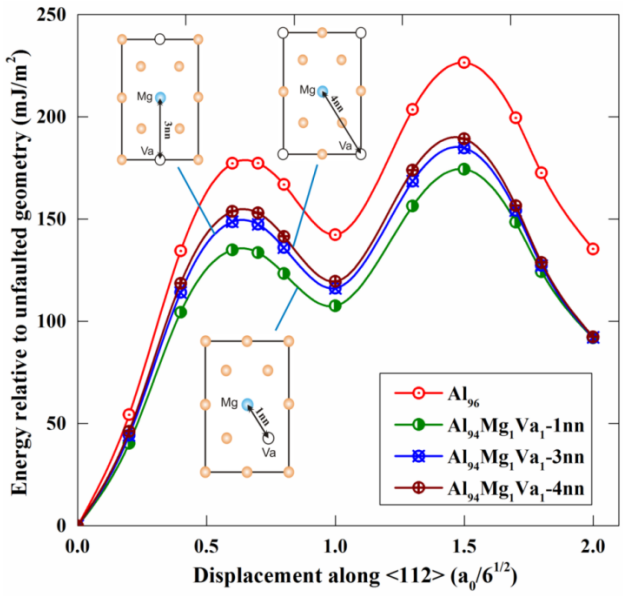

Fig. 6. The effect of Mg and vacancy pairs as 1st nearest neighbors (1nn), 3nn, and 4nn on the GPFE curves of Al. The Mg and vacancy occupation in the fault plane are as indicated.

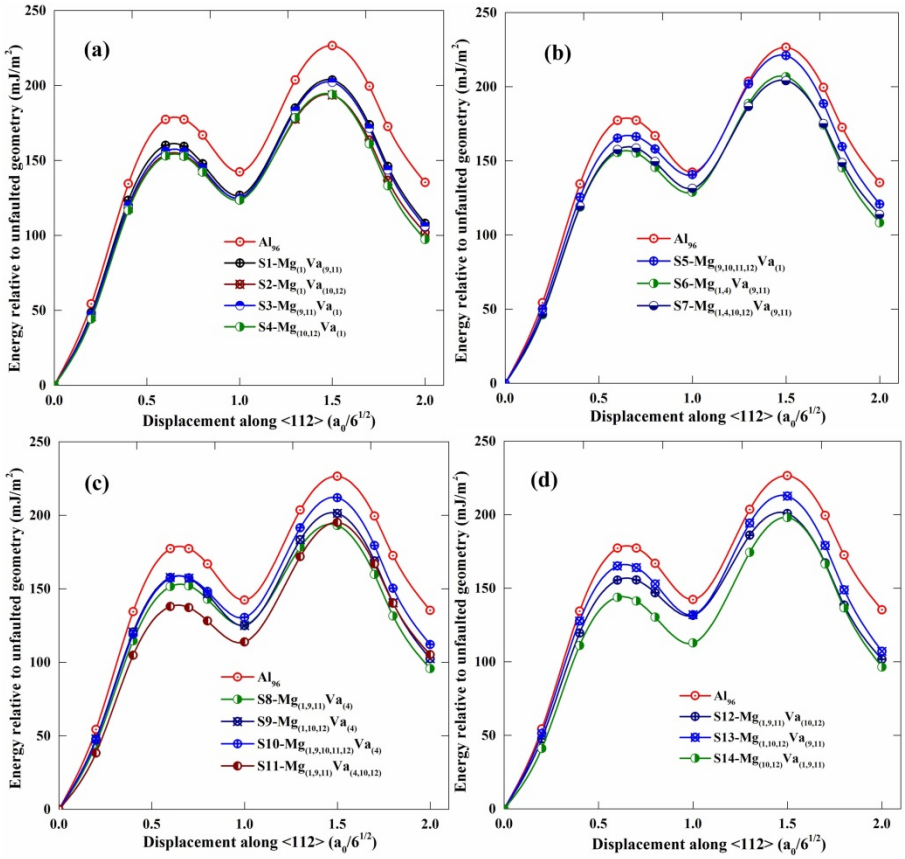

Fig. 7. Mg and vacancy complex effect on the GPFE curves of Al.

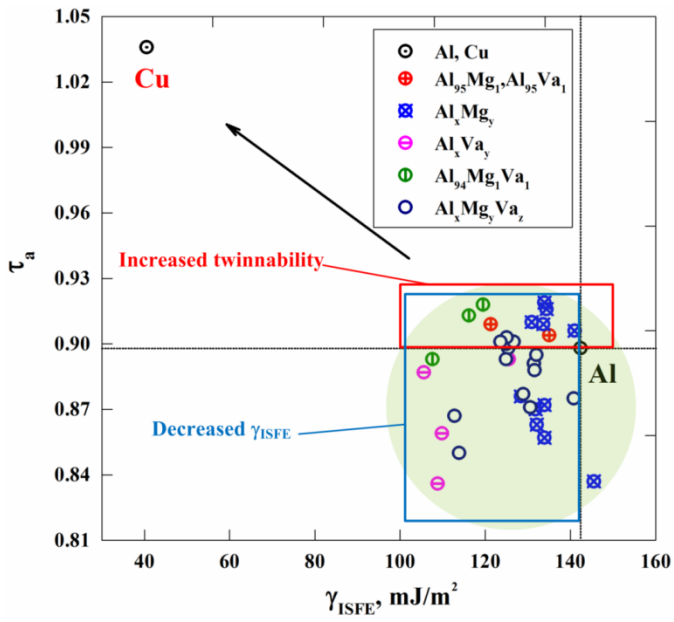

Fig. 8. Two dimensional τ_a-γ_{ISFE} map of all the investigated systems in the present work in comparison with Cu. The straight dot lines representing τ_a and γ_{ISFE} of Al are marked out. The increased twinnability as well as decreased γ_{ISFE} in comparison with Al are also as indicated.